

Bose–Einstein correlations in hadron-pairs from lepto-production on nuclei ranging from hydrogen to xenon

The HERMES Collaboration

A. Airapetian^{13,16}, N. Akopov²⁷, Z. Akopov⁶, E.C. Aschenauer⁷, W. Augustyniak²⁶, R. Avakian²⁷, A. Avetissian²⁷, E. Avetisyan⁶, S. Belostotski¹⁹, N. Bianchi¹¹, H.P. Blok^{18,25}, A. Borissov⁶, V. Bryzgalov²⁰, J. Burns¹⁴, M. Capiluppi¹⁰, G.P. Capitani¹¹, E. Cisbani²², G. Ciullo¹⁰, M. Contalbrigo¹⁰, P.F. Dalpiaz¹⁰, W. Deconinck⁶, R. De Leo², E. De Sanctis¹¹, M. Diefenthaler^{9,15}, P. Di Nezza¹¹, M. Düren¹³, G. Elbakian²⁷, F. Ellinghaus⁵, E. Etzelmüller¹³, R. Fabbri⁷, A. Fantoni¹¹, L. Felawka²³, S. Frullani²², G. Gapienko²⁰, V. Gapienko²⁰, J. Garay García^{4,6}, F. Garibaldi²², G. Gavrilo^{6,19,23}, V. Gharibyan²⁷, F. Giordano^{10,15}, S. Gliske¹⁶, M. Hartig⁶, D. Hasch¹¹, Y. Holler⁶, I. Hristova⁷, Y. Imazu²⁴, A. Ivanilov²⁰, H.E. Jackson¹, S. Joosten¹², R. Kaiser¹⁴, G. Karyan²⁷, T. Keri¹³, E. Kinney⁵, A. Kisselev¹⁹, V. Korotkov²⁰, V. Kozlov¹⁷, P. Kravchenko^{9,19}, V.G. Krivokhijine⁸, L. Lagamba², L. Lapikás¹⁸, I. Lehmann¹⁴, P. Lenisa¹⁰, A. López Ruiz¹², W. Lorenzon¹⁶, X.-G. Lu⁶, B.-Q. Ma³, D. Mahon¹⁴, N.C.R. Makins¹⁵, Y. Mao³, B. Marianski²⁶, A. Martinez de la Ossa⁶, H. Marukyan²⁷, Y. Miyachi²⁴, A. Movsisyan¹⁰, M. Murray¹⁴, A. Mussgiller^{6,9}, E. Nappi², Y. Naryshkin¹⁹, A. Nass⁹, M. Negodaev⁷, W.-D. Nowak⁷, L.L. Pappalardo¹⁰, R. Perez-Benito¹³, A. Petrosyan²⁷, P.E. Reimer¹, A.R. Reolon¹¹, C. Riedl^{7,15}, K. Rith⁹, G. Rosner¹⁴, A. Rostomyan⁶, J. Rubin^{15,16}, D. Ryckbosch¹², Y. Salomatin²⁰, A. Schäfer²¹, G. Schnell^{4,12}, B. Seitz¹⁴, T.-A. Shibata²⁴, V. Shutov⁸, M. Stahl¹³, M. Stancari¹⁰, M. Statera¹⁰, J.J.M. Steijger¹⁸, S. Taroian²⁷, A. Terkulov¹⁷, R. Truty¹⁵, A. Trzcinski²⁶, M. Tytgat¹², Y. Van Haarlem¹², C. Van Hulse^{4,12}, D. Veretennikov¹⁹, V. Vikhrov¹⁹, I. Vilardi², S. Wang³, S. Yaschenko^{6,9}, Z. Ye⁶, S. Yen²³, B. Zihlmann⁶, P. Zupranski²⁶

¹Physics Division, Argonne National Laboratory, Argonne, Illinois 60439-4843, USA

²Istituto Nazionale di Fisica Nucleare, Sezione di Bari, 70124 Bari, Italy

³School of Physics, Peking University, Beijing 100871, China

⁴Department of Theoretical Physics, University of the Basque Country UPV/EHU, 48080 Bilbao, Spain and IKERBASQUE, Basque Foundation for Science, 48013 Bilbao, Spain

⁵Nuclear Physics Laboratory, University of Colorado, Boulder, Colorado 80309-0390, USA

⁶DESY, 22603 Hamburg, Germany

⁷DESY, 15738 Zeuthen, Germany

⁸Joint Institute for Nuclear Research, 141980 Dubna, Russia

⁹Physikalisches Institut, Universität Erlangen-Nürnberg, 91058 Erlangen, Germany

¹⁰Istituto Nazionale di Fisica Nucleare, Sezione di Ferrara and Dipartimento di Fisica e Scienze della Terra, Università di Ferrara, 44122 Ferrara, Italy

¹¹Istituto Nazionale di Fisica Nucleare, Laboratori Nazionali di Frascati, 00044 Frascati, Italy

¹²Department of Physics and Astronomy, Ghent University, 9000 Gent, Belgium

¹³II. Physikalisches Institut, Justus-Liebig Universität Gießen, 35392 Gießen, Germany

¹⁴SUPA, School of Physics and Astronomy, University of Glasgow, Glasgow G12 8QQ, United Kingdom

¹⁵Department of Physics, University of Illinois, Urbana, Illinois 61801-3080, USA

¹⁶Randall Laboratory of Physics, University of Michigan, Ann Arbor, Michigan 48109-1040, USA

¹⁷Lebedev Physical Institute, 117924 Moscow, Russia

¹⁸National Institute for Subatomic Physics (Nikhef), 1009 DB Amsterdam, The Netherlands

¹⁹B.P. Konstantinov Petersburg Nuclear Physics Institute, Gatchina, 188300 Leningrad Region, Russia

²⁰Institute for High Energy Physics, Protvino, 142281 Moscow Region, Russia

²¹Institut für Theoretische Physik, Universität Regensburg, 93040 Regensburg, Germany

²²Istituto Nazionale di Fisica Nucleare, Sezione di Roma, Gruppo Collegato Sanità and Istituto Superiore di Sanità, 00161 Roma, Italy

²³TRIUMF, Vancouver, British Columbia V6T 2A3, Canada

²⁴Department of Physics, Tokyo Institute of Technology, Tokyo 152, Japan

²⁵Department of Physics and Astronomy, VU University, 1081 HV Amsterdam, The Netherlands

²⁶National Centre for Nuclear Research, 00-689 Warsaw, Poland

²⁷Yerevan Physics Institute, 375036 Yerevan, Armenia

Abstract. Bose–Einstein correlations of like-sign charged hadrons produced in deep-inelastic electron and positron scattering are studied in the HERMES experiment using nuclear targets of ^1H , ^2H , ^3He , ^4He , N, Ne, Kr, and Xe. A Gaussian approach is used to parametrize a two-particle correlation function determined from events with at least two charged hadrons of the same sign charge. This correlation function is compared to two different empirical distributions that do not include the Bose–Einstein correlations. One distribution is derived from unlike-sign hadron pairs, and the second is derived from mixing like-sign pairs from different events. The extraction procedure used simulations incorporating the experimental setup in order to correct the results for spectrometer acceptance effects, and was tested using the distribution of unlike-sign hadron pairs. Clear signals of Bose–Einstein correlations for all target nuclei without a significant variation with the nuclear target mass are found. Also, no evidence for a dependence on the invariant mass W of the photon-nucleon system is found when the results are compared to those of previous experiments.

Introduction

Hadron production in deep-inelastic scattering (DIS) of leptons off nuclei is a powerful tool to study the quark hadronization process. The distance scale over which a struck quark that received a sufficiently large energy-momentum transfer from an incident lepton develops into a colorless hadronic particle extends well beyond the size of a single nucleon. Therefore, the distribution of hadrons in the final state may be modified by interactions of the developing hadronic state with the nuclear medium outside the struck nucleon. In general, this intermediate state is some mixture of quarks and gluonic fields that have not reached their asymptotic (confined) states, and so any modification should depend on the evolution of that state. Similarly the fully formed hadron may still pass through the nuclear medium and be subject to rescattering processes (see, e.g., Ref. [1]).

One means of studying the final hadronic state is the use of Bose–Einstein correlations (BEC) in the distribution of bosons, in particular pions. These correlations arise from interference between different parts of the symmetrized wave function of identical bosons from incoherent sources. This well-known technique of *intensity* interferometry was first developed by Hanbury Brown and Twiss to measure stellar radii [2]. Its first use in particle physics, half a century ago, was to study the $p\bar{p}$ annihilation process [3, 4] with incident anti-protons of 1 GeV momentum. Since then many measurements of BEC have been performed in hadron-hadron scattering experiments. In addition, several studies of BEC in the e^+e^- annihilation process have been performed (see, e.g., Ref. [5]), especially by the LEP experiments. Measurements of BEC from deep-inelastic lepton scattering experiments are less abundant. The results from experiments using charged leptons as incident particles can be found in Refs. [6, 7, 8, 9, 10], while the results from neutrino experiments are found in Refs. [11, 12, 13]. Several reviews [5, 14, 15, 16] summarize the present theoretical and experimental knowledge of BEC. The theory of BEC in particle physics was originally developed in the papers of Kopylov and Podgoretskii [17, 18, 19] and Cocconi [20]. It should be noted that most of the theoretical work has focused on the understanding of BEC in heavy-ion collisions, in which a “fireball” source distribution, created by the collision roughly at rest involving many parton elementary interactions, decays into hadrons. Only a few

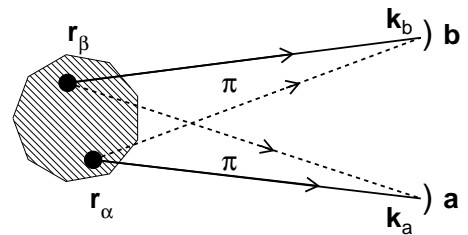


Fig. 1. Schematic illustration of the Bose–Einstein effect.

references consider the quite different case of fragmentation in DIS and e^+e^- processes, in which quite different hadron-momentum and spatial-source distribution might be assumed (see, e.g., Ref. [21, 22]). Estimates of BEC in e^+e^- annihilation from string-fragmentation models [22] indicate that correlation parameters are mostly dependent on string-breaking parameters, because the strongest correlations are from pions resulting from adjacent breaks along a string.

To better understand the underlying physics of BEC one may consider a simple example of the emission and detection of two identical bosons, e.g., two pions, from points \mathbf{r}_α and \mathbf{r}_β , which are observed with momenta \mathbf{k}_a and \mathbf{k}_b at detectors a and b (Fig. 1). The two pions are indistinguishable and the total wave function of the two-pion system must be symmetric under the exchange of them:

$$\Psi_{2\pi} = \frac{1}{\sqrt{2}} \left(\Psi_{a\alpha} \Psi_{b\beta} + \Psi_{b\alpha} \Psi_{a\beta} \right), \quad (1)$$

where $\Psi_{a\alpha}$ is the wave function of a pion produced at point \mathbf{r}_α and observed at detector a while $\Psi_{b\beta}$ is the wave function of a pion produced at point \mathbf{r}_β and observed at detector b . Assuming plane waves, i.e., $\Psi_{a\alpha} \approx \exp(i\mathbf{k}_a \cdot \mathbf{r}_\alpha)$, one may obtain $|\Psi_{2\pi}|^2 = 1 + \cos(\delta\mathbf{k} \cdot \delta\mathbf{r})$ with $\delta\mathbf{k} = \mathbf{k}_a - \mathbf{k}_b$ and $\delta\mathbf{r} = \mathbf{r}_\alpha - \mathbf{r}_\beta$. Thus the correlation function resulting from the interference of the two terms in Eq. (1) will take the following form:

$$R(\mathbf{k}_a, \mathbf{k}_b) \propto 1 + \cos(\delta\mathbf{k} \cdot \delta\mathbf{r}). \quad (2)$$

This expression shows that the BEC effect measures the projection of the spacial distance ($\delta\mathbf{r}$) between two particle sources on the direction of the momentum difference ($\delta\mathbf{k}$) between the observed pions. One can generalize two-point sources to a continuous space-time distribution of

sources. Experimentally this is achieved by finding the boson correlation function. In BEC this correlation observable is defined in terms of the two-particle correlation function

$$R(p_1, p_2) = D(p_1, p_2) / [D(p_1) \cdot D(p_2)], \quad (3)$$

where p_1 and p_2 are the particle four-momenta, $D(p_1, p_2)$ is the two-particle probability density and $D(p_1)$, $D(p_2)$ are one-particle probability densities.

Typical analyses use models for the correlation function R with a limited set of parameters. In the case of fireball decay (heavy-ion collision), the correlation function might be described by a (spherical) Gaussian distribution in space with an independent parametrized exponential decay in time. However, such an approach is not Lorentz invariant. Generally the Goldhaber parametrization [4] is a more convenient approach, in which the distribution is a function of the Lorentz-invariant quantity T^2 of the hadron pair, where $T^2 = -(p_1 - p_2)^2 = S - 4m_\pi^2$ with S the squared invariant mass of the pair and m_π the pion mass. In this parametrization the correlation function R takes the form

$$R(T) = 1 + \lambda \cdot e^{-T^2 r_G^2}. \quad (4)$$

This parametrization corresponds to a Gaussian shape of the particle source distribution of size r_G in the center of mass of the pair. The additional parameter λ , the chaoticity (or incoherence), has been introduced to account for a possible incoherent contribution of the pion emitters. Completely coherent pion sources lead to the absence of correlations among the bosons ($\lambda = 0$) [23, 24], while in the simplest theoretical treatment, completely incoherent sources lead to $\lambda = 1$. Subsequent theoretical work has shown that a number of different effects can modify the value of λ in both directions, greater and smaller than unity (see, e.g. Ref. [14]). Examples of such effects are the presence of decay products of long-lived resonances in addition to directly produced bosons in the final state, final-state interactions (FSI), and the deviation of the exact shape of the source distribution from the assumed Gaussian form. Other experimental effects can also influence the experimentally measured value of λ , often due to the purity of the boson sample as determined by the quality of the particle identification within the experiment. For these reasons, it is difficult to compare the results of λ between different experiments, even at identical kinematic conditions.

Note that the Goldhaber parametrization does not correspond to any well developed theoretical approach but rather serves as a convenient tool for the comparison of experimental results. The parametrization describes the shape of the distribution in T satisfactorily. However, depending on the physics of the reaction, a rigorous treatment of the coherent and incoherent sources requires modification of the functional form of the correlation function (see, e.g., Ref. [25]).

Given these remarks, one must note that there are additional points to consider in a full treatment of BEC. Initial correlations among the bosons are affected by FSI

between the produced particles as well as with the production environment, both via the Coulomb interaction and hadronic interactions. The long-range Coulomb FSI is quite often accounted for by introducing a multiplicative Gamow factor [23]. It increases (decreases) the two-particle density for opposite-(like-)sign particles. The correction factor is essential only at very small values of T and very quickly approaches unity with increasing T . For pion pairs at $T = 0.05$ GeV the correction factor differs from unity by only about 1.5%. There are other more elaborate calculations that predict an even smaller magnitude for the required correction and also examine its model dependence. Short-range strong FSI between the two identical pions may also influence their correlation (see, e.g., Ref. [5, 14, 15, 16, 26]); without clear theoretical estimates for the kinematics of the present experiment it was chosen not to attempt any correction for both long-range and short-range FSI.

Effects that can alter the pair correlation within the nuclear environment are the focus of this study of BEC for nuclear targets ranging from hydrogen to xenon. Measurements with the same experimental apparatus and kinematics help to minimize possible systematic bias in the observed target-mass dependence. In DIS a difference in the size of the particle emission region could exist for pions produced off a free nucleon as compared to that off bound nucleons. In addition, interactions of the struck bare quark, during fragmentation, or of the fully developed hadron with the nuclear environment could alter both the apparent size of the emission region and the amount of incoherence. For example, a common simple assumption is that the correlations of a pair of identical pions are determined by the relative positions of their last scattering points, which thereby play the role of independent particle sources. If the pions scatter from the nuclear matter, one would expect an increase in the size of the emission source as a function of target radius. Another example would be the increasing probability of gluon radiation within the nucleus leading to a change in the pion-pair correlations relative to hadronization in free space.

The influence of nuclear re-scattering processes on BECs in heavy-ion collisions was studied in Ref. [27] and effects on the source size of 15-20% were found. No estimates exist for the case of lepton-nucleus hadron production. Earlier experimental studies of BECs from DIS by nuclei are quite limited. The BBCN Collaboration [12] found the BEC parameters r_G and λ to be independent of the atomic mass. These measurements, however, are limited to three light nuclei, ^1H , ^2H , and Ne.

There is significant evidence that the nuclear medium affects the hadronization processes in lepton scattering at HERMES energies. Results on this subject have been presented in a number of papers [1, 28, 29, 30, 31, 32, 33, 34]. In particular, the transparency of the ^2H , ^3He , and ^{14}N nuclei to exclusive incoherent ρ^0 electro-production has been measured [28] and significant dependences on the coherence length were found. A series of papers [1, 29, 30, 31] is devoted to the investigation of the hadron multiplicity variation in different kinematic regions and

its dependence on the target atomic mass A up to xenon. The most prominent features of the data are an increased hadron attenuation with increasing value of the mass number A of the nucleus and the attenuation becoming smaller (larger) with increasing values of ν (z), where ν is the energy of the virtual photon in the laboratory system, and $z = E_h/\nu$ is the fractional hadron energy.

The influence of the nuclear medium on the ratio of double-hadron to single-hadron yields in DIS was also investigated [32]. Nuclear effects are clearly observed but with substantially smaller magnitude as well as reduced A dependence compared to the single-hadron multiplicity ratios. The first detailed study of the dependence on the target nuclear mass of the average squared transverse momentum $\langle p_t^2 \rangle$ of hadrons produced in deep-inelastic lepton scattering is described in [33]. It is found that the average squared transverse momentum is increasing with the atomic mass number.

In short, several studies with different nuclear targets performed at HERMES show significant modifications of the hadron observables within the nuclear medium as compared to the results on a proton/deuteron target.

Experiment

The present measurement of the BEC was performed with the HERMES spectrometer [35] using the 27.6 GeV polarized lepton (electron/positron) beam stored in the HERA ring at DESY. The spectrometer consisted of two identical halves above and below the lepton beam line. The scattered lepton and the produced hadrons were detected within an angular acceptance of ± 170 mrad horizontally, and $\pm(40-140)$ mrad vertically.

All the targets were internal to the lepton storage ring and consisted of polarized or unpolarized ^1H , ^2H , and ^3He , or unpolarized ^4He , N, Ne, Kr, or Xe gas injected into a thin-walled open-ended tubular storage cell. Target areal densities up to 1.4×10^{16} nucleons/cm² were obtained for unpolarized gas corresponding to luminosities up to 3×10^{33} cm⁻² s⁻¹. The luminosity was measured using elastic scattering of the beam leptons off the electrons in the target gas, Bhabha scattering for a positron beam and Møller scattering for an electron beam [36].

The trigger was formed by a coincidence between the signals from three scintillator hodoscope planes, and a lead-glass calorimeter where a minimum energy deposit of 3.5 GeV (1.4 GeV) for unpolarized (polarized) target was required. The scattered leptons were identified using a transition-radiation detector, a scintillator pre-shower counter, an electromagnetic calorimeter, and a threshold gas Cherenkov counter. In 1998 the threshold Cherenkov counter was replaced by a ring-imaging Cherenkov detector (RICH).

Analysis

Scattered leptons are selected by imposing constraints on the squared four-momentum of the virtual photon,

Table 1. Number of DIS events with more than one detected hadron, N_{ev} , the number of like-sign hadron pairs, N^{like} , and of unlike-sign hadron pairs, N^{unlike} , that meet the kinematic requirements for each target.

Nucleus	N_{ev}	N^{like}	N^{unlike}
^1H	1145046	478946	958185
^2H	1297356	680143	1178797
^3He	34391	15295	29165
^4He	79776	30539	59244
N	92968	41112	78402
Ne	175594	75898	146145
Kr	211456	91391	172946
Xe	106274	46130	87125

$Q^2 > 1$ GeV², and on the invariant mass of the photon-nucleon system, $W^2 > 10$ GeV². The constraint on W^2 is applied in order to ensure the predominance of multiple particle production in the DIS events.

The results of this study are based on data collected by the HERMES Collaboration between the years 1996 and 2006. The yields from polarized targets are summed over both target spin orientations. The yields from all targets are summed over both (longitudinal) beam polarization states.

Events with only one identified lepton of the same charge as the beam lepton and momentum larger than 3.5 GeV are accepted. The presence of at least two charged hadrons with momenta $2.0 \text{ GeV} < p_h < 15 \text{ GeV}$ is required for further analysis. The total numbers of such multi-hadron DIS events, N_{ev} , the numbers of like-sign, N^{like} , and unlike-sign, N^{unlike} , hadron pairs available for the analysis are given in Table 1 for each target.

In this analysis all charged hadrons are considered to be pions. Simulations using the PYTHIA 6.2 event generator [37], tuned to provide an accurate description [38] of semi-inclusive deep-inelastic hadron lepto-production in the HERMES kinematic region, show that the observed charged hadrons are distributed in relative proportion $\pi/K/p(\bar{p}) = 78\%/12\%/10\%$. In the same simulations one finds that 55% of like-sign hadron pairs and 66% of unlike-sign hadron pairs are truly pion pairs. This results in a “dilution” of the parameter λ under the assumption that the non-pion pairs do not contribute to the BEC. The value of λ in this analysis is expected to be smaller than about 0.5. Kaon like-sign pairs contribute only 2% while their unlike-sign pairs contribute about 4%.

Experimentally, it is difficult to measure the inclusive single particle spectrum required to determine the probability density $D(p)$ for all possible momenta p in the formal definition of the correlation function $R(p_1, p_2)$. A common practice is to substitute the two one-particle probability distributions $D(p_1) \cdot D(p_2)$ with a two-particle probability density reference distribution $D_r(p_1, p_2)$. This reference distribution is constructed from experimental two-particle distributions that do not have any BECs.

The experimental correlation function is then defined as

$$R(p_1, p_2) = D(p_1, p_2)/D_r(p_1, p_2). \quad (5)$$

The Goldhaber parametrization usually used includes an additional normalization parameter γ and a polynomial function $\mathcal{P}(T)$ to describe the long-range correlations at large T and has the form

$$R(T) = \gamma \cdot [1 + \lambda \cdot e^{-T^2 r_G^2}] \cdot \mathcal{P}(T). \quad (6)$$

The long-range correlations at large T may appear due to charge and energy conservation, phase-space constraints and imperfections in the reference sample. The form of the polynomial $\mathcal{P}(T)$ used to model these long-range correlation effects is taken to be $(1 + \delta \cdot T^2)$. A linear dependence $(1 + \delta' \cdot T)$ is used to estimate the influence of the chosen form on the final results. The parameter δ and δ' are free parameters like r_G , λ , and γ .

The magnitude of the two-particle BEC is measured by comparison of the experimental distribution with a reference sample distribution [see Eq. (5)]. The method of constructing the reference sample is the main source of systematic uncertainty, especially since the multiplicity of hadrons in the HERMES experiment is relatively low. One of the main problems in measuring BEC is the evaluation of biases caused by an imperfect reference sample, thus it is desirable to use at least two different approaches to construct a reference sample to cross-check the correlation results.

Two of the most widely used methods to construct a reference sample are employed here:

- Method of event mixing (*MEM*),
- Method of unlike-sign pairs (*MUS*).

In *MEM* hadron-pair distributions of the same charge are created by using hadrons from different events, while in *MUS* hadrons with different charge from the same event are used. Other methods can be found in the literature, each with its own shortcomings. The main technical difficulty of the two methods chosen here is the violation of momentum and energy conservation in the kinematic event topology when selecting two hadrons from different events in the case of *MEM*, and the contribution of events from resonances that are not present in the like-sign distribution in the case of *MUS*. The systematic effects associated with these two reference samples are studied using the PYTHIA-based Monte Carlo simulation of the HERMES experiment discussed above, the inclusion of quantum interference of BEC not being enabled in the PYTHIA event generation.

The construction of the reference sample using the *MUS* is done by forming the distribution in T of all unlike-sign hadron pairs, requiring the same constraints as for the like-sign pairs. For the *MEM*, to construct a sample of uncorrelated hadron pairs, a combination of charged hadrons from two different DIS events is used. The first hadron of a pair is taken from one event while the second hadron is taken from another event. Care must be taken to conserve collinearity of the virtual-photon

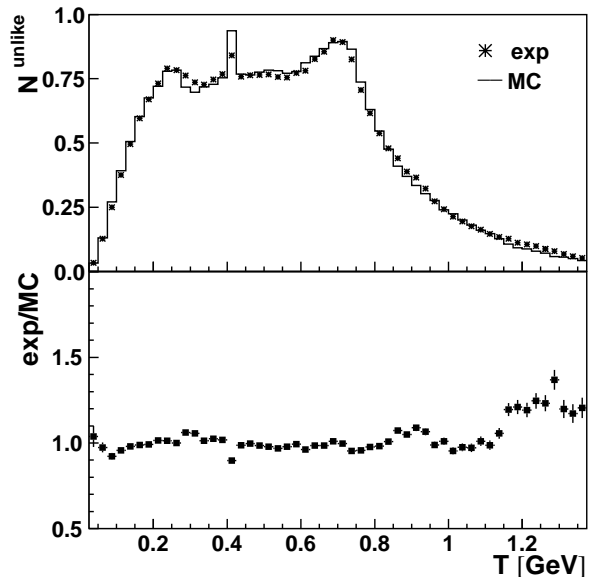


Fig. 2. Top panel: normalized experimental (stars) and simulated (line) distributions for unlike-sign hadron pairs as a function of the variable T . Bottom panel: the ratio of these experimental (exp) and simulated (MC) distributions.

vectors \mathbf{q}_1 and \mathbf{q}_2 from these two different events. For each event, the momentum vector of the total hadronic system must lie in the direction of the virtual photon $\mathbf{q} = \mathbf{p}_e - \mathbf{p}'_e$, where \mathbf{p}_e and \mathbf{p}'_e are the momenta of the incident and scattered leptons. To conserve collinearity the momenta of all hadrons in the second event must be rotated in such a way that the total hadronic momentum is aligned along the direction of \mathbf{q}_1 of the first event.

The quality of the HERMES simulation with respect to the description of the measured unlike-sign hadron pair distribution is demonstrated in Fig. 2 for a sample of hydrogen target data. The top panel shows the experimental T distribution of unlike-sign hadron pairs (exp) in comparison with the simulated data for h^+h^- pairs (MC). The bottom panel shows their ratio. The figure demonstrates good agreement between the experimental and simulated distributions. Based on this agreement, the simulation results are used to further reduce the systematic biases of the reference sample and experimental distributions through the use of a double-ratio definition for the correlation function $R(T)$. For the two methods in this analysis,

$$\begin{aligned} R^{MEM} &= (like/mixed)^{exp} / (like/mixed)^{MC}, \\ R^{MUS} &= (like/unlike)^{exp} / (like/unlike)^{MC}. \end{aligned} \quad (7)$$

Dividing the experimental ratios by the simulated ratios is expected to reduce biases resulting from the violation of kinematic constraints in the *MEM* and from resonance contamination in the *MUS*, since these biases also exist in the simulated event distributions.

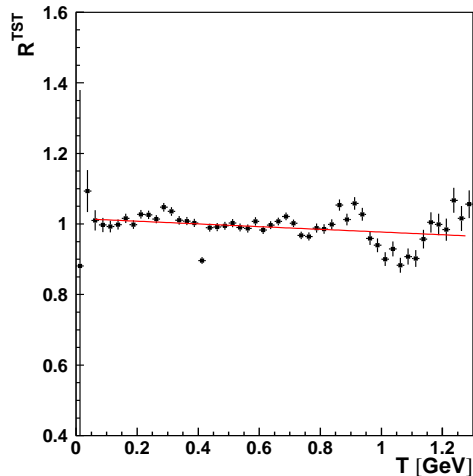


Fig. 3. Consistency check of the two chosen reference samples. The quantity R^{TST} is defined in the text. The curve is a linear fit to the data for T between 0.05 GeV and 1.3 GeV.

As a test of the validity of $R(T)$ using the simulation results with a double ratio, the *MEM* was used with unlike-sign hadron pairs from the hydrogen data sample to construct the double ratio

$$R^{TST} = (\text{unlike}/\text{mixed})^{\text{exp}} / (\text{unlike}/\text{mixed})^{\text{MC}}, \quad (8)$$

shown as a function of T in Fig. 3. This test ratio is expected to have no BECs, and ideally would have a value of unity over the entire T range. At very low T (≤ 0.05 GeV), at $T \approx 0.4$ GeV, and at $T > 0.9$ GeV this double ratio deviates from unity significantly. As shown by a linear fit to R^{TST} there is a slight linear dependence over most of the range of T , indicating some small residual bias. The deviation near 0.4 GeV in the simulation is likely due to insufficient description of K_S production, which contributes to the N^{unlike} distributions (see Fig. 2). The deviations at very low and at large T likely arise from some combination of effects in both the simulation of the *MUS* and the *MEM* construction of the reference sample. The very low T region, $T < 0.05$ GeV, of the double ratio distributions is excluded from further analysis due to lack of statistics. A fit to the correlation function R^{TST} (shown in Fig. 3) with the Goldhaber parametrization [Eq. (6)] over the range $0.05 \text{ GeV} < T < 1.30 \text{ GeV}$ gives $\lambda = 0.000 \pm 0.003$ and $r_G = 0.0 \pm 1.4$ fm, suggesting that the fluctuations at large T and the slight non-zero linear dependence on T do not cause a significant bias of the extracted parameters λ and r_G .

Results

The double-ratio correlation functions obtained from hydrogen data are shown in Fig. 4 for both types of the reference sample. The curves in the figure are results of fits using the Goldhaber parametrization [Eq. (6)]. The

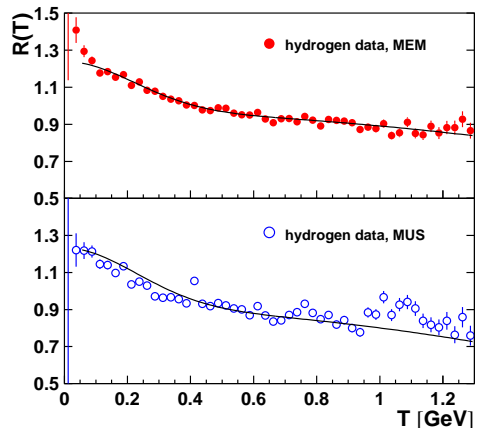


Fig. 4. Double ratio correlation function for like-sign hadron pairs obtained with *MEM* and *MUS* based on hydrogen target data.

fits are performed over the range of $0.05 \text{ GeV} < T < 1.30 \text{ GeV}$. The values for the two parameters obtained from the fits are given in Table 2.

The systematic uncertainties are estimated by variations of the fit range in T , the bin width, and the polynomial form for the long-range correlations term, i.e., using a linear dependence $(1 + \delta'T)$. The results of the two different methods are consistent (see Table 2). Values of the fit parameter δ from the quadratic form of $\mathcal{P}(T)$ are -0.08 ± 0.01 and -0.05 ± 0.01 respectively for the *MEM* and *MUS*.

The kinematic dependence of the BEC parameters on the invariant mass W of the photon-nucleon system has been studied for the hydrogen target data sample. In Fig. 5 the resulting parameters r_G and λ are presented for like-sign hadron pairs as a function of W obtained with the *MEM* and *MUS* methods. Within the present systematic and statistical uncertainties there is no clear dependence of the parameters on the invariant mass W in this range. Previous measurements from the HERA H1 experiment [8] over a broad range at high W ($65 \text{ GeV} <$

Table 2. Results for the Goldhaber parametrization fitted to the HERMES hydrogen data, both for the mixed-event method (*MEM*) and the method of unlike-sign pairs (*MUS*).

Method	Goldhaber parameters
<i>MEM</i>	$r_G = 0.64 \pm 0.03(\text{stat})^{+0.04}_{-0.04}(\text{sys})$ fm $\lambda = 0.28 \pm 0.01(\text{stat})^{+0.00}_{-0.05}(\text{sys})$
<i>MUS</i>	$r_G = 0.72 \pm 0.04(\text{stat})^{+0.09}_{-0.09}(\text{sys})$ fm $\lambda = 0.28 \pm 0.02(\text{stat})^{+0.02}_{-0.04}(\text{sys})$

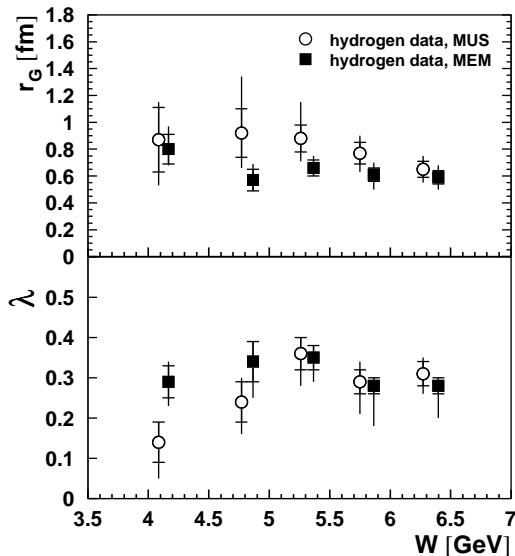


Fig. 5. Parameter r_G (top panel) and λ (bottom panel) as a function of W , obtained with *MEM* and *MUS* methods on hydrogen. The inner and outer error bars indicate the statistical and total uncertainties. For the latter the statistical and systematic uncertainties are added in quadrature.

$W < 240$ GeV) found only slight evidence of an increase in r_G .

As mentioned above, BEC has been studied in a number of lepton-hadron and e^+e^- experiments. The Goldhaber parametrization is used in most of these analyses. The parameter r_G as a function of the average value of W in lepton-nucleon scattering experiments is shown in Fig. 6. The parameter λ for a given experiment may depend on the hadron fractions and on the experimental details, hence the results of λ obtained here are not compared to those in other measurements. In the majority of these experiments the extracted values of r_G depend upon the method of the construction of the reference sample. Even for a single experiment, e.g., EMC, the parameter r_G obtained with the *MUS* is twice as large as that obtained with *MEM*. From Fig. 6 no clear dependence of the parameter r_G on W can be deduced, from neither methods (*MEM* and *MUS*). The following conclusions are drawn from a comparison of these results from the different experiments:

1. Most values of the parameter r_G are in the range of 0.4 fm to 1.0 fm.
2. The results strongly depend on the choice of the reference sample. Analyses of the same data set with different reference samples often give incompatible results for r_G (and λ).
3. The *MUS* typically gives higher values for the parameter r_G than the *MEM*.

The HERMES results on hydrogen are in general agreement with those of previous lepton-nucleon scattering experiments over a broad range in W , and agree well with the BBCN neutrino experiment, which is at a slightly

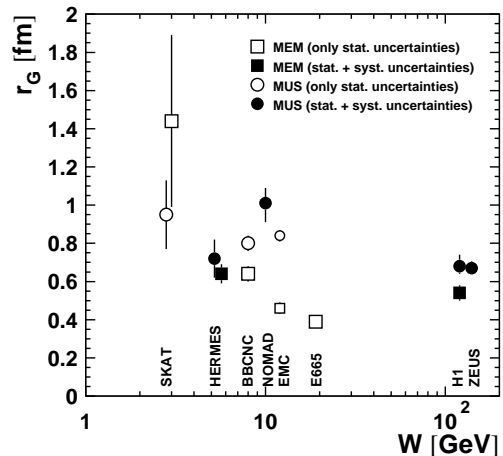


Fig. 6. Goldhaber radius r_G , as a function of W , obtained in lepton nucleon scattering experiments [6, 7, 8, 9, 11, 12, 13]. Different markers are used to indicate the different methods for the construction of the reference sample and the kinds of uncertainties included.

higher mean W than HERMES. Similar results are seen in e^+e^- collisions at LEP (see Ref. [5]).

A possible nuclear dependence in BEC was examined using an extensive HERMES data set (cf. Table 1). The correlation function for like-sign hadron pairs produced in scattering off the nuclear targets ^2H , ^3He , ^4He , N, Ne, Kr, and Xe was determined using the same approximate parametrization as given in Eq. 6. Systematic uncertainties are estimated separately for each target and each reference sample (*MEM* and *MUS*). The parameters r_G and λ are presented in Fig. 7 as a function of the target atomic mass A . No dependence of these parameters on target atomic mass is observed within the estimated uncertainties. Fit results with a constant over the whole range of the atomic mass for the four sets of data points are presented in Table 3. Here, the total uncertainty of each particular point is taken as the quadratic sum of statistical and systematic uncertainties. The parameters extracted with the two reference samples are in good agreement.

Table 3. Fit of a constant to the Goldhaber parameters as a function of the target atomic mass A . Results are given for both the mixed-event method (*MEM*) and the method of unlike-sign pairs (*MUS*).

Method	Value	χ^2/NDF
<i>MEM</i>	$r_G = 0.634 \pm 0.017$ fm	1.5
	$\lambda = 0.289 \pm 0.006$	2.1
<i>MUS</i>	$r_G = 0.636 \pm 0.021$ fm	1.2
	$\lambda = 0.289 \pm 0.011$	1.4

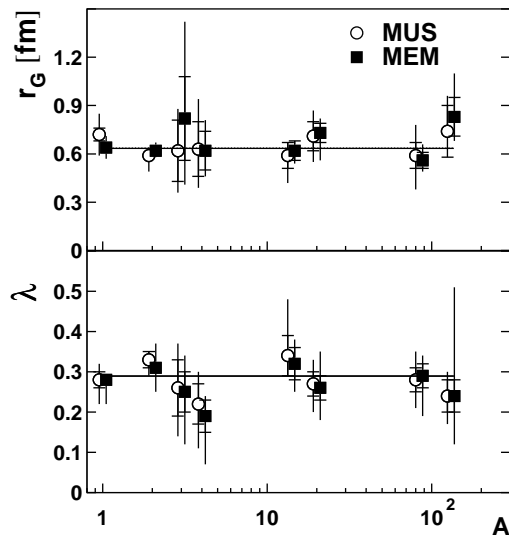


Fig. 7. The parameters r_G (top panel) and λ (bottom panel) are shown as a function of the target atomic mass A . The inner part of the error bars indicate the statistical uncertainty and the total error bars have systematic uncertainties added in quadrature. The horizontal lines correspond to the average value of the parameters.

To date there are no theoretical estimates for the magnitude of nuclear effects on BEC in DIS. In the absence of some hitherto unknown effect of multi-particle correlations, hadrons produced are expected to interact with the nuclear medium. Within the sensitivity of this experiment no clear dependence of the parameters λ and r_G on the target atomic mass is observed, consistent with earlier results by the BBCN Collaboration [12]. This is similar to the rather weak dependence of the double-hadron yields on the target atomic mass observed at HERMES [32], in contrast to much stronger effects observed in the distributions of single-hadron yields [1, 29, 30, 31].

In conclusion, a study of the Bose–Einstein correlations between two like-sign hadrons produced in semi-inclusive deep-inelastic electron/positron scattering off nuclear targets ranging from hydrogen to xenon has been carried out. Two different methods of constructing the reference sample are used in this study, and Bose–Einstein correlations are clearly observed in all the data samples. The results obtained using the two reference sample methods are in good agreement, suggesting that most of the systematic uncertainties connected with the construction of the reference samples are taken into account by the use of double ratios corrected via an accurate experimental simulation. Within the total experimental uncertainties, no dependence of the parameters r_G and λ on the target atomic mass is observed.

We gratefully acknowledge the DESY management for its support and the staff at DESY and the collaborating institutions for their significant effort. This work was supported by the

Ministry of Education and Science of Armenia; the FWO-Flanders and IWT, Belgium; the Natural Sciences and Engineering Research Council of Canada; the National Natural Science Foundation of China; the Alexander von Humboldt Stiftung, the German Bundesministerium für Bildung und Forschung (BMBF), and the Deutsche Forschungsgemeinschaft (DFG); the Italian Istituto Nazionale di Fisica Nucleare (INFN); the MEXT, JSPS, and G-COE of Japan; the Dutch Foundation for Fundamenteel Onderzoek der Materie (FOM); the Russian Academy of Science and the Russian Federal Agency for Science and Innovations; the Basque Foundation for Science (IKERBASQUE) and the UPV/EHU under program UFI 11/55; the U.K. Engineering and Physical Sciences Research Council, the Science and Technology Facilities Council, and the Scottish Universities Physics Alliance; as well as the U.S. Department of Energy (DOE) and the National Science Foundation (NSF).

References

1. HERMES Collaboration, A. Airapetian *et al.*, Nucl. Phys. B **780**, 1 (2007).
2. R. Hanbury Brown and R.Q. Twiss, Nature **178**, 1046 (1956).
3. G. Goldhaber, W.B. Fowler, S. Goldhaber, T.F. Hoang, Phys. Rev. Lett. **3**, 181 (1959).
4. G. Goldhaber, S. Goldhaber, W. Lee, A. Pais, Phys. Rev. **120**, 300 (1960).
5. G. Alexander, Rep. Prog. Phys. **66**, 481 (2003).
6. EMC, M. Arneodo *et al.*, Zeit. Phys. C **32**, 1 (1986).
7. E665 Collaboration, M.R. Adams *et al.*, Phys. Lett. B **308**, 418 (1993).
8. H1 Collaboration, C. Adloff *et al.*, Zeit. Phys. C **75**, 437 (1997).
9. ZEUS Collaboration, S. Chekanov *et al.*, Phys. Lett. B **583**, 231 (2004).
10. ZEUS Collaboration, S. Chekanov *et al.*, Phys. Lett. B **652**, 1 (2007).
11. SKAT Collaboration, V.V. Ammosov *et al.*, Sov. J. Nucl. Phys. **53**, 609 (1991).
12. BBCN Collaboration, V.A. Korotkov *et al.*, Zeit. Phys. C **60**, 37 (1993).
13. NOMAD Collaboration, P. Astier *et al.*, Nucl. Phys. B **686**, 3 (2004).
14. R.M. Weiner, Phys. Rept. **327**, 249 (2000).
15. W. Kittel, Acta Phys. Polonica B **32**, 3927 (2001).
16. K. Zalewski, arXiv:hep-ph/0607222.
17. G.I. Kopylov, M.I. Podgoretskii, Sov. J. Nucl. Phys. **15**, 219 (1972).
18. G.I. Kopylov, Phys. Lett. B **50**, 472 (1974).
19. G.I. Kopylov, M.I. Podgoretskii, Sov. J. Nucl. Phys. **18**, 336 (1974).
20. G. Cocconi, Phys. Lett. B **49**, 459 (1974).
21. J.D. Bjorken, Lect. Notes Phys. **56**, 93 (1976).
22. B. Andersson and W. Hofmann, Phys. Lett. B **169**, 364 (1986).
23. M. Gyulassy, S.K. Kauffmann, and L.W. Wilson, Phys. Rev. C **20**, 2267 (1979).
24. M.G. Bowler, Zeit. Phys. C **29**, 617 (1985).
25. K. Geiger, J. Ellis, U. Heinz, and U.A. Wiedemann, Phys. Rev. D **61**, 054002 (2000).

26. M.G. Bowler, *Zeit. Phys. C* **46**, 305 (1990).
27. J.I. Kapusta and Y. Li, *Phys. Rev. C* **72**, 064902 (2005).
28. HERMES Collaboration, A. Airapetian *et al.*, *Phys. Rev. Lett.* **82**, 3025 (1999).
29. HERMES Collaboration, A. Airapetian *et al.*, *Eur. Phys. J. C* **20**, 479 (2001).
30. HERMES Collaboration, A. Airapetian *et al.*, *Phys. Lett. B* **577**, 37 (2003).
31. HERMES Collaboration., A. Airapetian *et al.*, *Eur. Phys. J. A* **47**, 113 (2011).
32. HERMES Collaboration, A. Airapetian *et al.*, *Phys. Rev. Lett.* **96**, 162301 (2006).
33. HERMES Collaboration, A. Airapetian *et al.*, *Phys. Lett. B* **684**, 114 (2010).
34. HERMES Collaboration, A. Airapetian *et al.*, *Phys. Rev. D* **90**, 072007 (2014).
35. HERMES Collaboration, K. Ackerstaff *et al.*, *Nucl. Instrum. Methods A* **417**, 230 (1998).
36. T. Benisch *et al.*, *Nucl. Instrum. Methods A* **471**, 314 (2001).
37. T. Sjöstrand *et al.*, *Comput. Phys. Commun.* **135**, 238 (2001).
38. P. Liebing, Ph.D. thesis, University of Hamburg (2004), DESY-THESIS-2004-036.